Electronic Supplementary Material (ESI) for ChemComm.

Acceptor-induced cooperative supramolecular co-assembly with emissive charge-transfer for supramolecular encryption

Zhao Gao,[a] Fei Yan,[a] Shuai Qiu,[a] Yifei Han,[b] Feng Wang[b] and Wei Tian[a]*

[a]Shaanxi Key Laboratory of Macromolecular Science and Technology, MOE Key Laboratory of Material Physics and Chemistry under Extraordinary conditions, School of Chemistry and Chemical Engineering, Northwestern Polytechnical University, Xi'an, 710072, P. R. China. E-mail: happytw_3000@nwpu.edu.cn.
[b]CAS Key Laboratory of Soft Matter Chemistry, iChEM (Collaborative Innovation Center of Chemistry for Energy Materials), Department of Polymer Science and Engineering, University of Science and Technology of China, Hefei, Anhui 230026, P. R. China.

Supporting Information

1. Materials and methods

9,10-diiodoanthracene,[S1] compounds **1**,[S2] and **4** [S3] (see Scheme S1 and S2) were synthesized according to the previously reported literatures. Other reagents and solvents used in the experiments were purchased from the commercial sources without further purification.

^{1}H NMR and ^{13}C NMR spectra were obtained from Bruker Avance 400 instruments. Matrix-assisted laser desorption/ionization time-of-flight mass spectrometry mass (MALDI-TOF-MS) measurements were recorded on a Bruker Autoflex Speed spectrometer with DCTB as the matrix. UV–Vis spectra were performed on a Shimadzu UV-2550 spectrometer. Fluorescence spectra were recorded on a Hitachi F-4600 FL spectrophotometer. The absolute fluorescence quantum yield (Φ_F) and time-resolved fluorescence lifetime experiments were recorded on an Edinburgh FLS980 transient steady-state fluorescence spectrometer. Φ_F was measured using a calibrated integrating sphere. Fourier transform infrared (FTIR) spectra were performed on a Nicolet iS50 infrared spectrometer. Transmission electron microscope (TEM) images were recorded on a JEM-2100 electron microscope. Dynamic light scattering (DLS) experiments were conducted on a Brookhaven BI-9000AT instrument. Solid-state ^{13}C NMR spectra were recorded on a JEOL JNM-ECZ400R/S1 instrument.

Theoretical calculations: all of the optimized structures were performed on G09 software packages.[S4] All of the elements were described by the B3LYP/6-31G(d) computational method. There are no imagery frequencies for the optimized geometries.

Mathematical fitting of the supramolecular co-assembly processes: the co-assembly of **G1/TCNB** is described using the nucleation-elongation cooperative model, which was developed by Meijer, *et al*.[S5] This model is used to describe the co-assembly of **G1/TCNB** which exhibits a non-sigmoidal melting curve as shown in the temperature-dependent UV–Vis experiments. In terms of **G2/TCNB**, a sigmoidal curve is obtained by plotting the fraction of aggregated species (α_{agg}) against temperature, revealing the involvement of isodesmic co-assembly mechanism.[S6] To acquire detailed thermodynamic parameters for the co-assembly processes of **G1/TCNB** and **G2/TCNB**,

the normalized UV–Vis melting curves obtained by plotting α_{agg} (λ = 568 nm for **G1/TCNB**, and 489 nm for **G2/TCNB**) against temperature are fitted with the respective mathematical model. In addition, the data of solvent-dependent UV–Vis absorption spectra for **G1/TCNB** can be fitted with the solvent-dependent equilibrium model reported by the previous literature.[S7]

Inkjet printing experiments: the printing experiments were performed on a commercially available inkjet printer (HP Deskjet 2131) with the customized HP803 black inkjet cartridge. The original black inks from the cartridge were removed, and the cartridge was washed with ethanol, water and dried with N_2 blowing. The inks of **G1** (0.5 mL, 1.0 mM) and **TCNB** (0.5 mL,1.0 mM) were then loaded separately into the clean black cartridge to perform the printing experiments.

*2. Supramolecular self-assembly behaviors of **Gn** (n=0−2)*

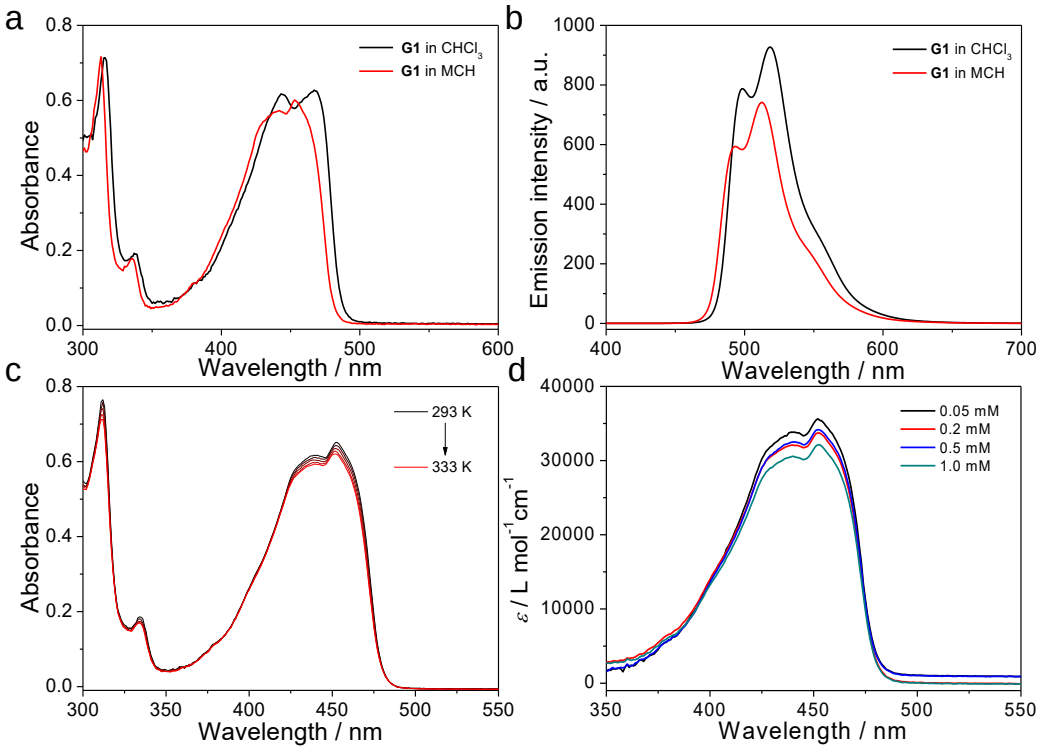

Figure S1. (a) UV−Vis and (b) fluorescence spectra of **G1** (2.0×10^{-5} M) in $CHCl_3$ and MCH. λ_{ex} = 453 nm. (c) Temperature-dependent UV–Vis spectra of **G1** (2.0×10^{-5} M) in MCH. (d) Concentration-dependent UV–Vis spectra of **G1** in MCH (from 1.0×10^{-3} M to 5.0×10^{-5} M, 298 K). When switching the solvent from polar $CHCl_3$ to nonpolar MCH, the maximum absorption band of **G1** is blue-shifted, whilst the band remains nearly unaltered in the temperature- and concentration- dependent UV–Vis spectra experiments. Such phenomena suggest a weak aggregation for **G1** in the current situations.

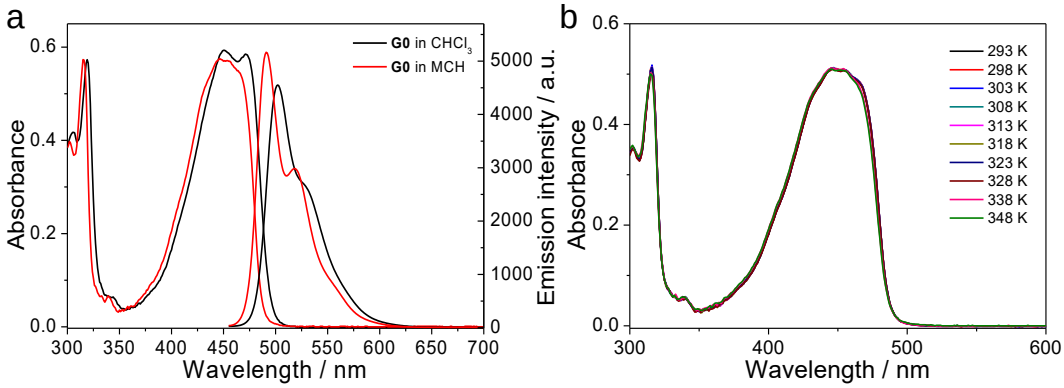

Figure S2. (a) UV−Vis and fluorescence spectra of **G0** (2.0×10^{-5} M) in $CHCl_3$ and MCH. λ_{ex} = 446 nm. (b) Temperature-dependent UV–Vis spectra of **G0** (2.0×10^{-5} M) in MCH.

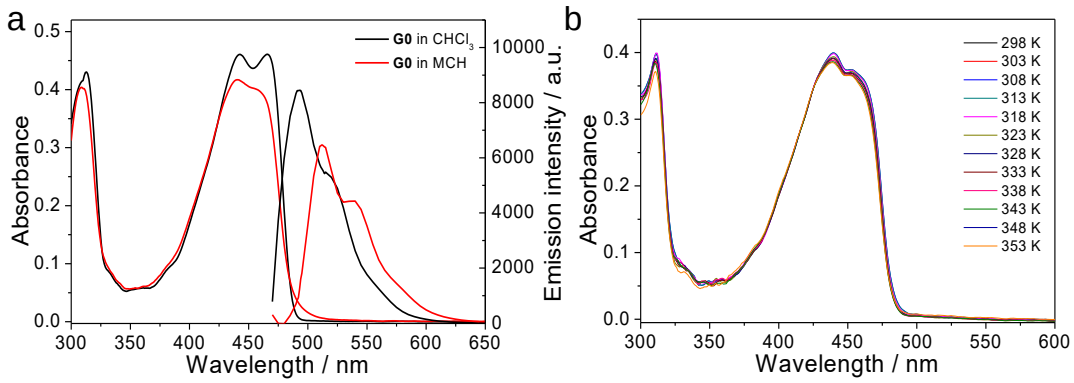

Figure S3. (a) UV−Vis and fluorescence spectra of **G2** (2.0×10^{-5} M) in $CHCl_3$ and MCH. λ_{ex} = 442 nm. (b) Temperature-dependent UV–Vis spectra of **G2** (2.0×10^{-5} M) in MCH.

*3. Supramolecular co-assembly behaviors of **Gn** (n=0−2) with **TCNB***

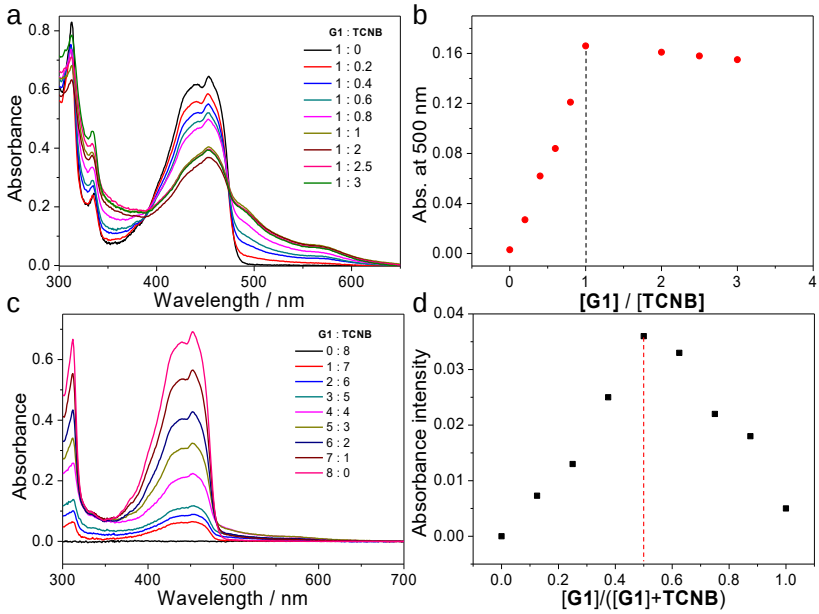

Figure S4. (a) UV−Vis absorbance changes upon gradual addition of **TCNB** into **G1** (2.0×10^{-5} M) in MCH. (b) The intensity changes at λ=500 nm. (c)−(d) Job's plot between **G1** and **TCNB** ([**G1**] + [**TCNB**] = 2.0×10^{-5} M), by plotting the intensity changes of UV−Vis absorbance band at 500 nm against the mole fraction of **G1**. Upon progressive addition of **TCNB** into the MCH solution of **G1**, the absorption band centred at 453 nm gradually decreases, whilst a broad and relatively lower-energy band locating between 500 and 625 nm emerges. The red-shifted band reaches to the maximum when adding equivalent **TCNB**, which suggests a 1 : 1 binding stoichiometry between **G1** and **TCNB**. Moreover, the Job's plot experiments also demonstrate the 1 : 1 stoichiometry of the complex **G1**/**TCNB**.

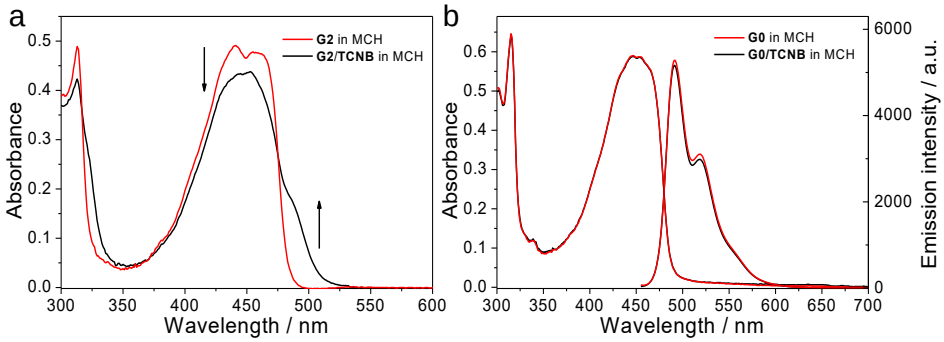

Figure S5. UV−Vis and fluorescence spectra of (a) **G2** (2.0×10^{-5} M) and **G2**/**TCNB** (2.0×10^{-5} M for each component) in MCH, and (b) **G0** (2.0×10^{-5} M) and **G0**/**TCNB** (2.0×10^{-5} M for each component) in MCH. For the second-generation dendrimer **G2**, a new shoulder band between 477 and 525 nm emerges after mixing equivalent **G2** and **TCNB** together, which arises from the charge transfer (CT) interaction from donor **G2** to acceptor **TCNB**. In stark contrast, the CT process cannot occur between the zeroth-generation dendrimer **G0** and **TCNB**, as evidenced by the almost no changes of UV−Vis and fluorescence signals in MCH.

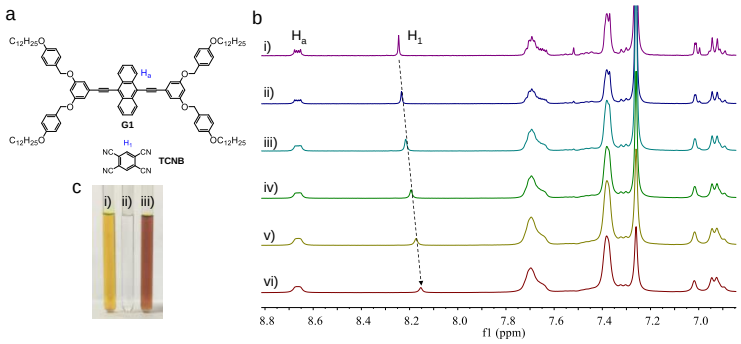

Figure S6. a) Molecular structures of **G1** and **TCNB**. b) Concentration-dependent ^{1}H NMR spectra (400 MHz, 298 K) of **G1**/**TCNB** in $CDCl_3$: (i) 1.0 mM, (ii) 2.0 mM, (iii) 4.0 mM, (iv) 6.0 mM, (v) 8.0 mM, and (vi) 10.0 mM. c) Photographs of i) **G1**, ii) **TCNB**, iii) **G1**/**TCNB** in concentrated $CDCl_3$ solution (10.0 mM for each component).

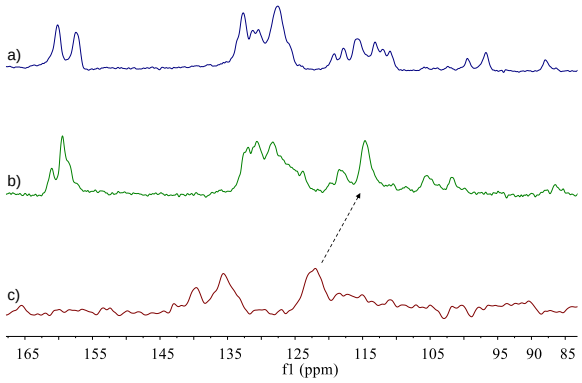

Figure S7. Solid-state ^{13}C NMR of **G1**, **G1**/**TCNB**, and **TCNB**. Solid-state ^{13}C NMR measurements are performed to determine the change of C atom chemical circumstances. The chemical shift of **G1** at around 110–120 ppm shifts downfield, and that of **TCNB** at 122 ppm shifts to 115 ppm, which indicate the reduction of π-electron density on **G1** and the increase of electron density of benzene ring on **TCNB**.

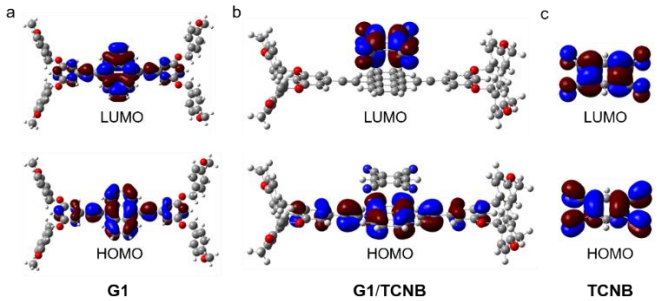

Figure S8. Molecular orbital diagrams of (a) **G1**, (b) **G1**/**TCNB**, and (c) **TCNB** *via* TD-DFT computation. The highest occupied molecular orbital (HOMO) of **G1**/**TCNB** is nearly completely localized on the electron-donor **G1**, whilst the lowest unoccupied molecular orbital (LUMO) is distributed on the acceptor **TCNB**, which indicates the electron transition from HOMO of donor to LUMO of acceptor.

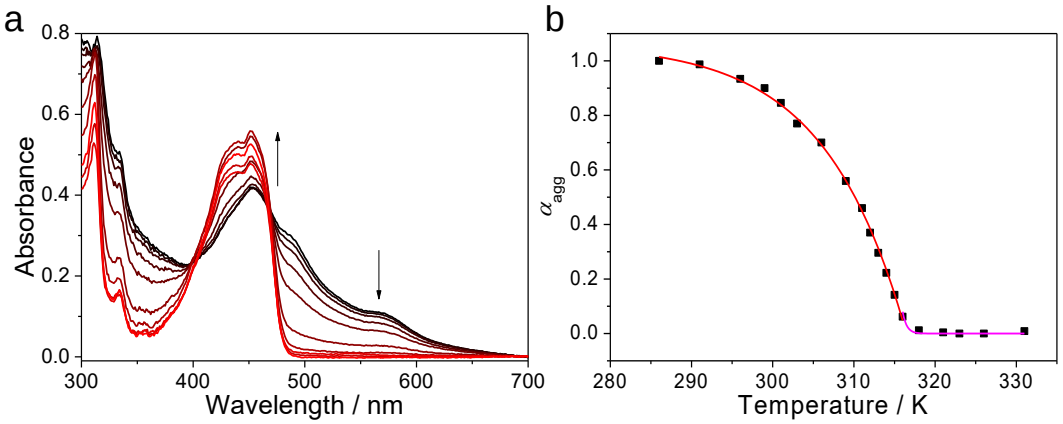

Figure S9. (a) Temperature-dependent UV−Vis spectra of **G1**/**TCNB** (2.0×10^{-5} M) in MCH. Arrows indicate the spectral variations upon increasing temperature. (b) α_{agg} of **G1**/**TCNB** (on the basis of CT band at 568 nm) *versus* temperature in MCH. The obtained data feature a non-sigmoidal curve, denoting the adoption of nucleation–elongation cooperative mechanism. The solid lines denote the mathematical fitting of the curve according to the Meijer–Schenning–Van-der-Schoot model.

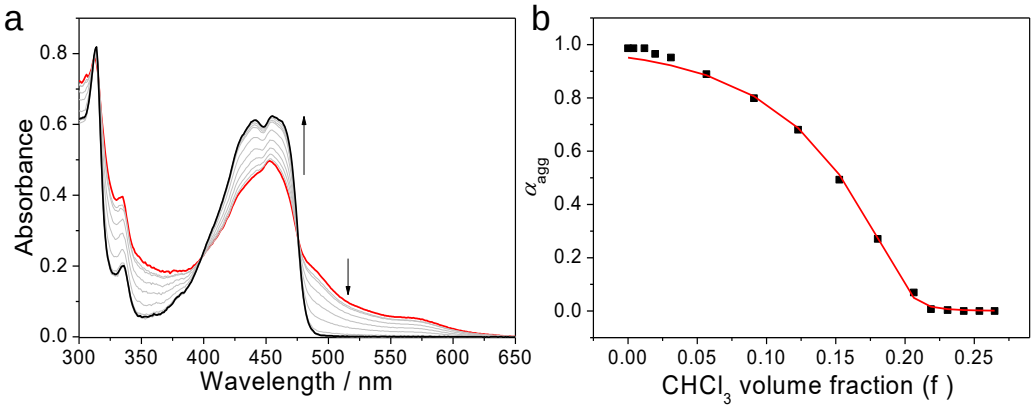

Figure S10. (a) Solvent-dependent UV–Vis spectra of **G1**/**TCNB** (2.0×10^{-5} M). Arrows indicate the spectral changes upon increasing $CHCl_3$ volume fraction (*f*) in MCH. (b) α_{agg} as a function of *f* monitored at 500 nm. The red line denotes the mathematical fitting of the curve according to the solvent-dependent equilibrium model. The cooperativity parameter (σ) is determined to be 1.9×10^{-3}, demonstrating the involvement of a cooperative mechanism for the co-assembly process of **G1**/**TCNB**.

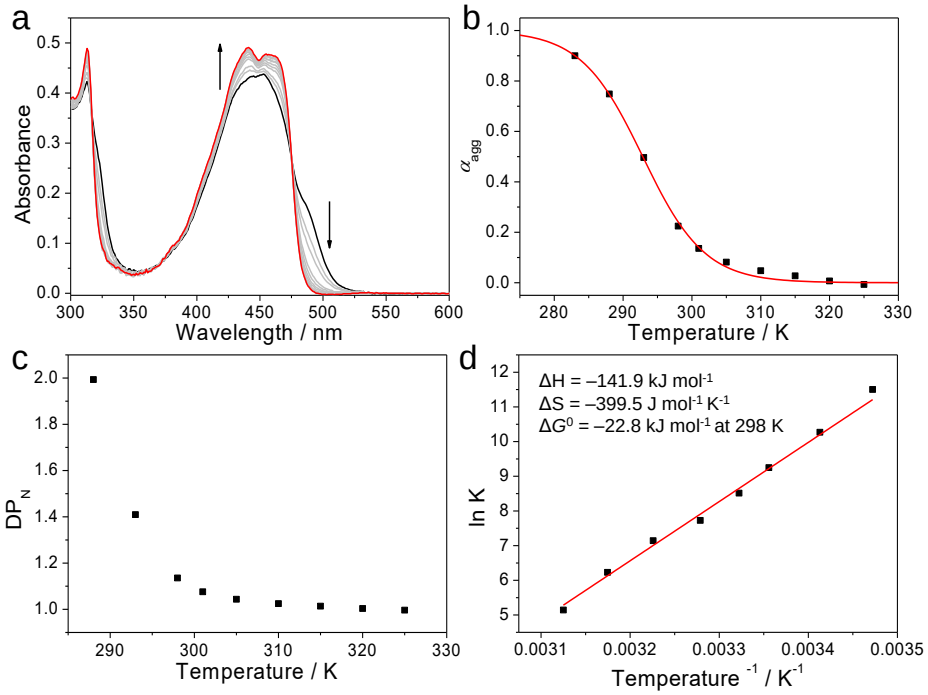

Figure S11. (a) Temperature-dependent UV−Vis spectra of **G2**/**TCNB** (2.0×10^{-5} M) in MCH. Arrows indicate the spectral variations upon increasing temperature. (b) α_{agg} of **G2**/**TCNB** (on the basis of CT band at 489 nm) *versus* temperature. The red line represents the non-linear fitting of the data according to the isodesmic mathematical model. c) Number-averaged degree of polymerization (DP_N) of **G2**/**TCNB** at different temperatures. d) Van't Hoff plot for the temperature dependence of the aggregation constant (K) of **G2**/**TCNB** in MCH. The sigmoidal melting curve obtained from the temperature-dependent UV−Vis spectra of **G2**/**TCNB** can be nicely fitted by the isodesmic model, which indicates the adoption of the isodesmic mechanism of the co-assembly process. According to the Van't Hoff plot, ΔG^0 of **G2**/**TCNB** was calculated to be –22.8 kJ mol^{-1} at 298 K, which is lower than that of **G1**/**TCNB** (–36.0 kJ mol^{-1}).

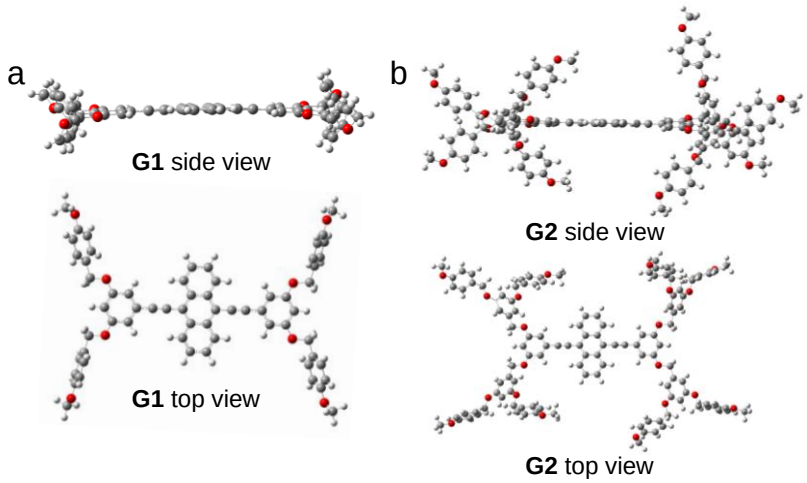

Figure S12. Optimized geometries of structures a) **G1** and b) **G2**, on the basis of DFT calculations at the level of B3LYP/6-31G(d).

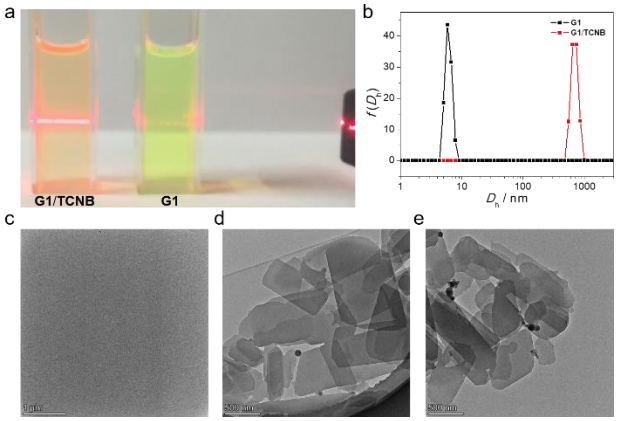

Figure S13. (a) Photographs of the MCH solution of **G1** (2.0×10^{-5} M) and **G1**/**TCNB** (2.0×10^{-5} M) irradiating with a laser pen. (b) DLS measurements of **G1** and **G1**/**TCNB** in MCH. TEM micrographs of (c) **G1** and (d)−(e) **G1**/**TCNB** on the copper grids. No aggregation can be detected for **G1** in MCH, which is manifested by the results of no Tyndall effect, small DLS hydrodynamic diameter, and no morphology in TEM. The results are coincident with that of UV−Vis and fluorescence spectra measurements. When adding equivalent **TCNB** into the MCH solution of **G1**, the co-assembly **G1**/**TCNB** is prone to assemble into large-sized nanosheets, with the averaged hydrodynamic diameter of 750 nm.

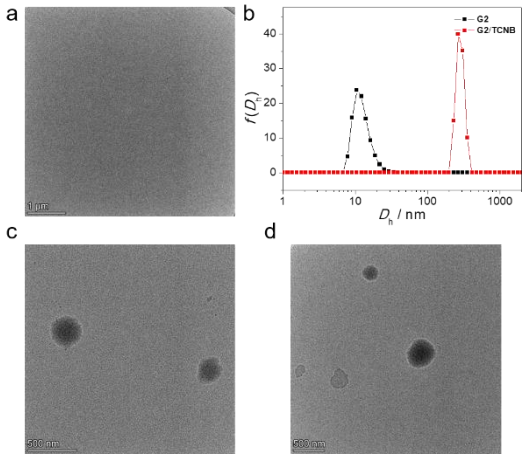

Figure S14. (a) TEM micrograph of **G2**. (b) DLS measurements of **G2** (2.0×10^{-5} M) and **G2**/**TCNB** (2.0×10^{-5} M) in MCH. (c)−(d) TEM micrographs of **G2**/**TCNB**. No microstructures can be detected for **G2**. In comparison, **G2**/**TCNB** is prone to assemble into nanoparticles with 265 nm in diameter.

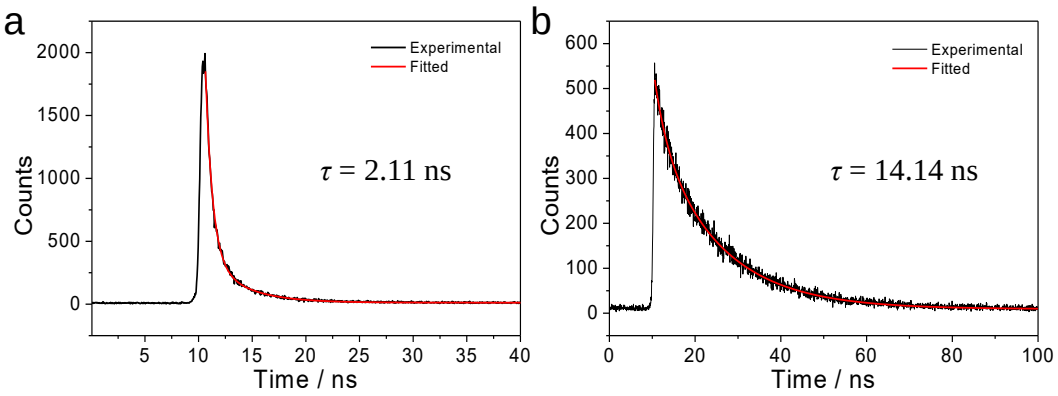

Figure S15. Fluorescence decay profiles of (a) **G1** film (λ_{ex} = 454 nm, λ_{em} = 552 nm) and (b) **G1**/**TCNB** film (λ_{ex} = 500 nm, λ_{em} = 619 nm).

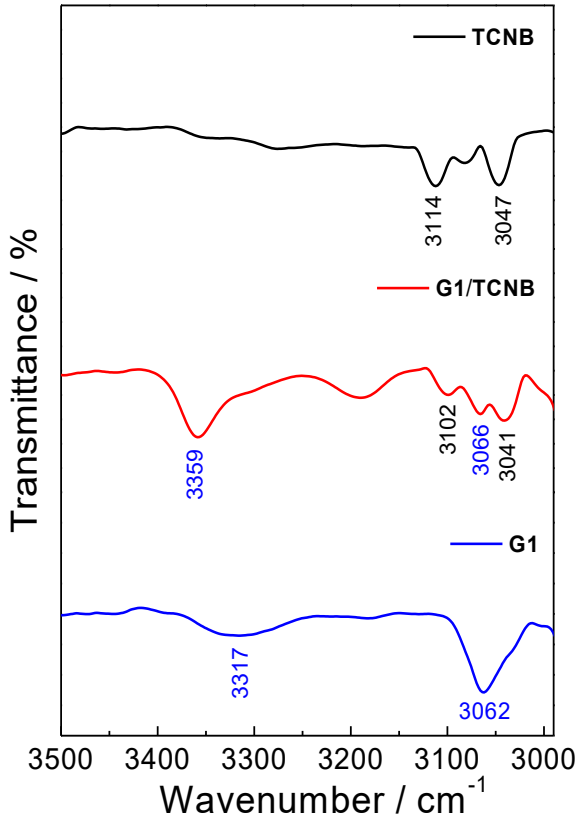

Figure S16. FTIR spectra of **G1**, **TCNB** and **G1**/**TCNB**. Depending on the FTIR measurements, the bands at 3114 and 3047 cm^{-1} (C−H str) of **TCNB** slightly shift to the lower frequency of 3102 and 3041 cm^{-1} in **G1**/**TCNB**, respectively, which are ascribed to the CT interaction from **G1** to **TCNB**.

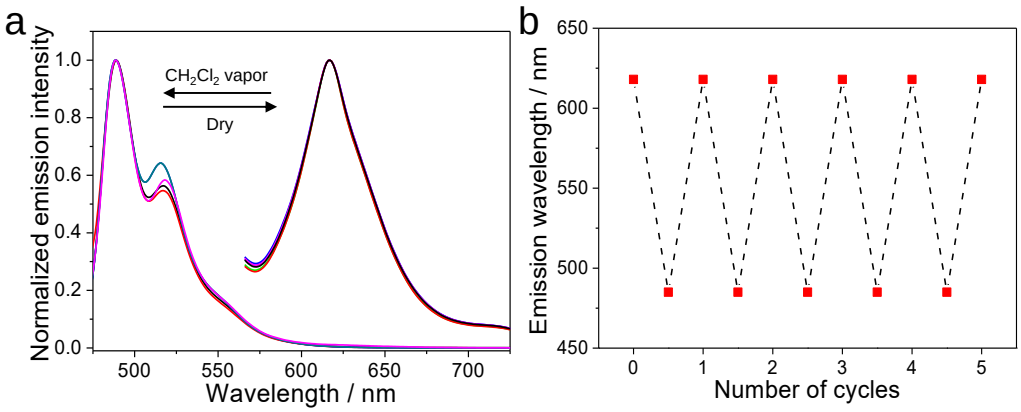

Figure S17. (a) Fluorescence spectra and (b) wavelength changes for the film of **G1**/**TCNB** as a function of CH_2Cl_2 vapor/dry cycles. Upon successively fuming with CH_2Cl_2 vapor and drying at room temperature, the emission signals of **G1**/**TCNB** can be reversibly switched for multiple cycles.

*4. Supramolecular encryption applications of **G1/TCNB***

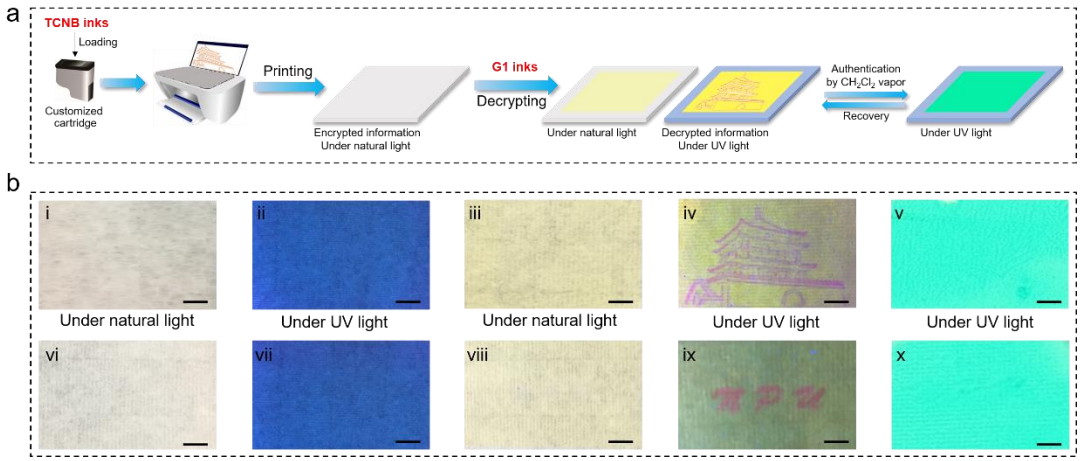

Figure S18. (a) Schematic illustration for **G1/TCNB** toward supramolecular encryption applications. (b) Digital photographs of the luminescent image at different stages. Scale bars: 5 mm. A cartoon pattern of "Bell Tower" is firstly printed on a non-fluorescent paper, which is in the encrypted state because it is invisible under both natural and UV light (Fig. S16b, i and ii). After the paper is printed with **G1** inks, the pre-printed pattern is still invisible under natural light, but appears with red emission color under UV light (Fig. S16b, iii and iv). Notably, the decrypted information could be authenticated by CH_2Cl_2 vapor, as evidenced by the emission color variation as well as the vanishment of the pattern (Fig. S16b, v). Subsequently, the red emission pattern could fully restore after the paper is drying. Besides, some other pattern can also be designed derived from **G1/TCNB** for supramolecular encryption applications (Fig. S16b, vi–x).

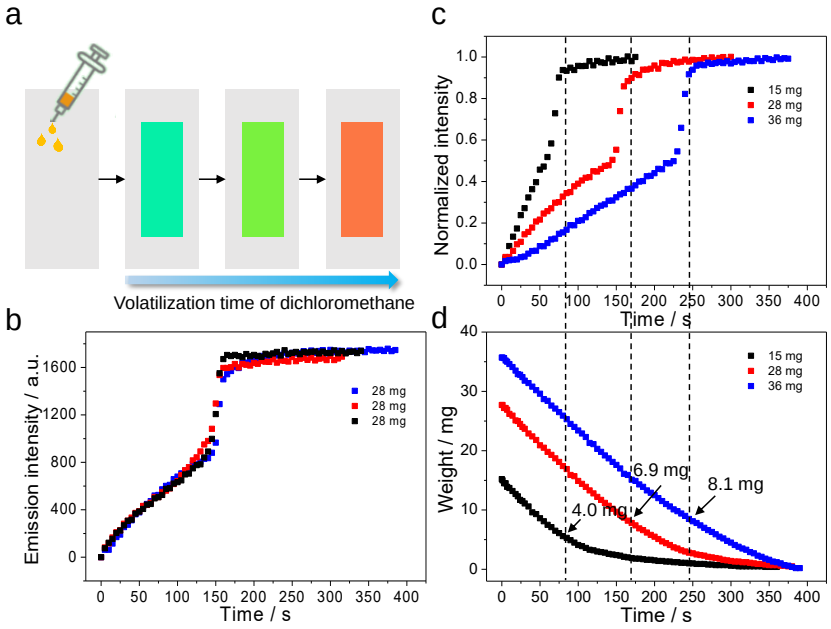

Figure S19. a) Schematic illustration of the sample preparation for quantitatively determining the molar stoichiometry of CH_2Cl_2 in the vapo-fluorochromic experiments. b) Fluorescence spectra change of the prepared **G1/TCNB** samples (28 mg of **G1/TCNB** CH_2Cl_2 solution)

versus the volatilization time of CH_2Cl_2 at room temperature (λ_{ex} = 500 nm, λ_{em} = 620 nm). The black, red and blue dots represent three repeated experiments. c) Fluorescence spectra and d) weight changes of the three sets of prepared **G1**/**TCNB** samples *versus* the volatilization time of CH_2Cl_2 at room temperature. An elaborate experiment is designed to quantitatively determine the equivalent ratio of CH_2Cl_2 to **G1**/**TCNB** in the encryption/decryption process. Specifically, a small amount of **G1**/**TCNB** CH_2Cl_2 solution (2.6 mg/mL) is firstly dropping onto a filter paper. Upon slowly volatilizing the CH_2Cl_2 vapor in air at room temperature, the emission color turns from green to red. Time-dependent fluorescence spectra are then employed to probe the emissive CT band variations of **G1**/**TCNB** *versus* the volatilization time of CH_2Cl_2. In Figure S19b, the emission signal at 620 nm gradually increases, then sharply reach to a plateau at around 170 s (the experiment is repeated three times), indicating the residual CH_2Cl_2 solvent at this time is the necessary minimum amount for the vapo-fluorochromic experiments. Simultaneously, the weight change of the prepared **G1**/**TCNB** sample *versus* the volatilization time of CH_2Cl_2 is proceeded under the same conditions (Figure S19d). At 170 s, the weight of the residual CH_2Cl_2 solvent is measured to be around 6.9 mg (Figure S19d, red dots), which is 126 times the weight of **G1**/**TCNB**. Additionally, two sets of similar experiments are performed, by separately dropping 15 mg and 36 mg of **G1**/**TCNB** CH_2Cl_2 solution (2.6 mg/mL) onto the filter papers (Figure S19c and S19d, black and blue dots). The equivalent ratio of CH_2Cl_2 to **G1**/**TCNB** is determined to be 115 and 133 times, respectively.

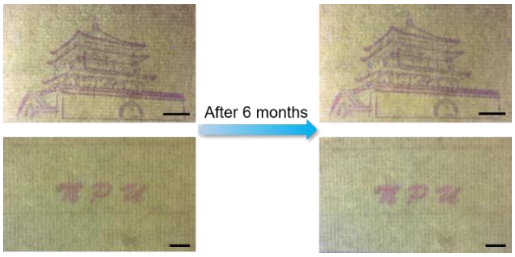

Figure S20. Photographs of the inkjet-printed fluorescent pattern on day 1 and after 6 months. The printed pattern derived from **G1**/**TCNB** features enough stability, as evidenced by unchanging of the emission color under the ambient conditions for at least 6 months.

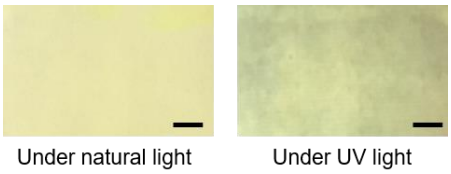

Figure S21. Digital photographs of the cartoon pattern of "Bell Tower" firstly printed with **TCNB** as inks and then printed with **G0** inks. Scale bars: 5 mm. As a control experiment, when **G0** is utilized in place of **G1** as fluorescent inks to decrypt the printed information, no distinguishable pattern emerges on the paper under both natural and UV light.

*5. Synthetic routes to dendrimers **Gn** (n=0−2)*

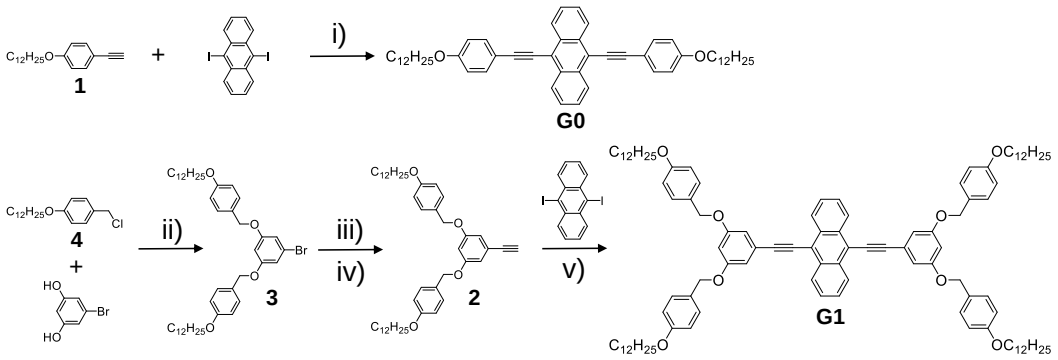

Scheme S1. Synthetic routes to the dendrimers **G0** and **G1**. i) $Pd(PPh_3)_2Cl_2$, CuI, TEA; ii) K_2CO_3, DMF; iii) trimethylsilylacetylene, $Pd(PPh_3)_2Cl_2$, CuI, TEA; iv) tetrabutylammonium fluoride, THF; v) $Pd(PPh_3)_2Cl_2$, CuI, TEA.

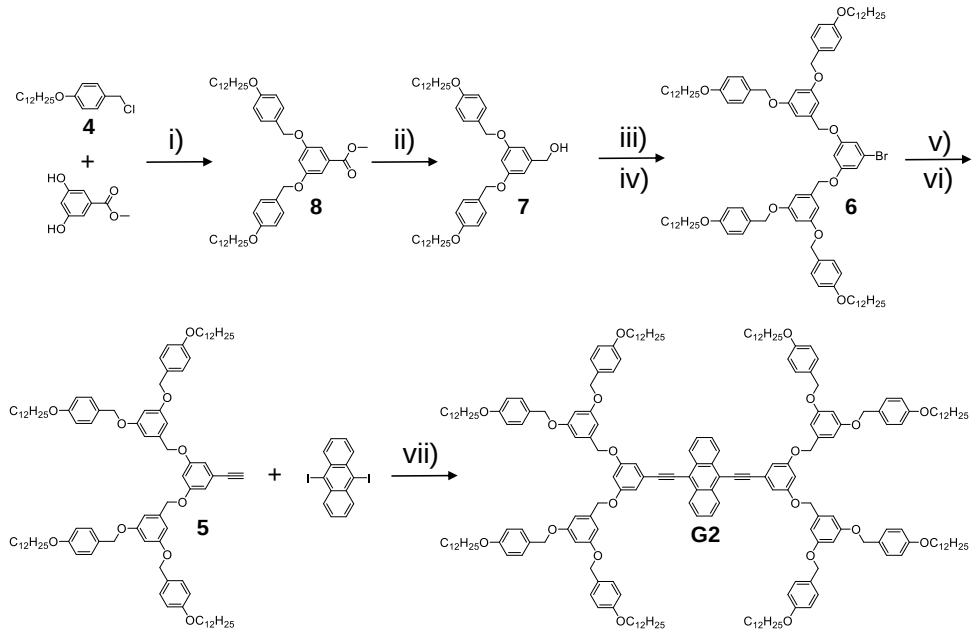

Scheme S2. Synthetic routes to the dendrimer **G2**. i) K_2CO_3, DMF; ii) $LiAlH_4$, THF; iii) $SOCl_2$, DCM; iv) 5-bromoresorcinol, $CsCO_3$, MeCN; v) 2-methyl-3-butyn-2-ol, $Pd(PPh_3)_2Cl_2$, CuI, TEA; vi) KOH, toluene; vii) $Pd(PPh_3)_2Cl_2$, CuI, TEA.

*5.1 Synthesis of dendrimer **G0***

9,10-diiodoanthracene (120 mg, 0.28 mmol), compound **1** (200 mg, 0.70 mmol)，$Pd(PPh_3)Cl_2$ (19.6 mg, 0.08 mmol) and CuI (5.33 mg, 0.03 mmol) were stirred in TEA (20 mL) and stirred under nitrogen atmosphere. After stirring at 75 °C for 12 hours, the reaction mixture was evaporated to remove the solvent, and the residue was extracted with H_2O/CH_2Cl_2 for three times. The combined organic extracts were dried over

anhydrous Na_2SO_4, and the solvent was removed with a rotary evaporator. The residue was purified by flash column chromatography (petroleum ether/CH_2Cl_2, 5 : 1 *v*/*v* as the eluent) to afford **G0** as an orange solid (172 mg, 82 %). ^{1}H NMR (400 MHz, $CDCl_3$) δ (ppm): 8.69 (dd, J = 6.6, 3.3 Hz, 4H), 7.70 (d, J = 8.8 Hz, 4H), 7.63 (dd, J = 6.7, 3.2 Hz, 4H), 6.97 (d, J = 8.8 Hz, 4H), 4.03 (t, J = 6.6 Hz, 4H), 1.82 (dd, J = 14.7, 6.8 Hz, 4H), 1.51–1.45 (m, 4H), 1.28 (s, 32H), 0.89 (t, J = 6.8 Hz, 6H). ^{13}C NMR (101 MHz, $CDCl_3$) δ (ppm): 159.80, 133.18, 132.15, 127.39, 126.58, 118.63, 115.60, 114.97, 102.68, 85.45, 68.38, 31.94, 29.67, 29.65, 29.61, 29.59, 29.41, 29.34, 29.30, 26.09, 22.68, 14.02. MALDI-TOF-MS *m*/*z*: $[M + H]^+$, $C_{54}H_{67}O_2$, calculated 747.5141; found 747.5199.

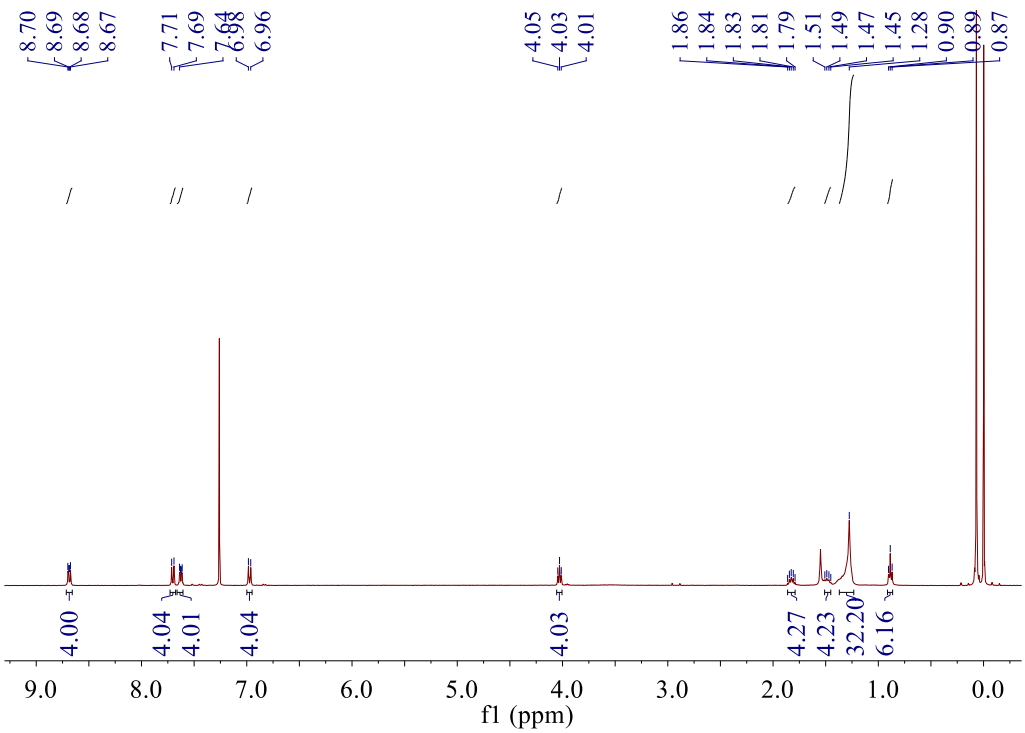

Figure S22. ^{1}H NMR spectrum (400 MHz, $CDCl_3$, 298K) of **G0**.

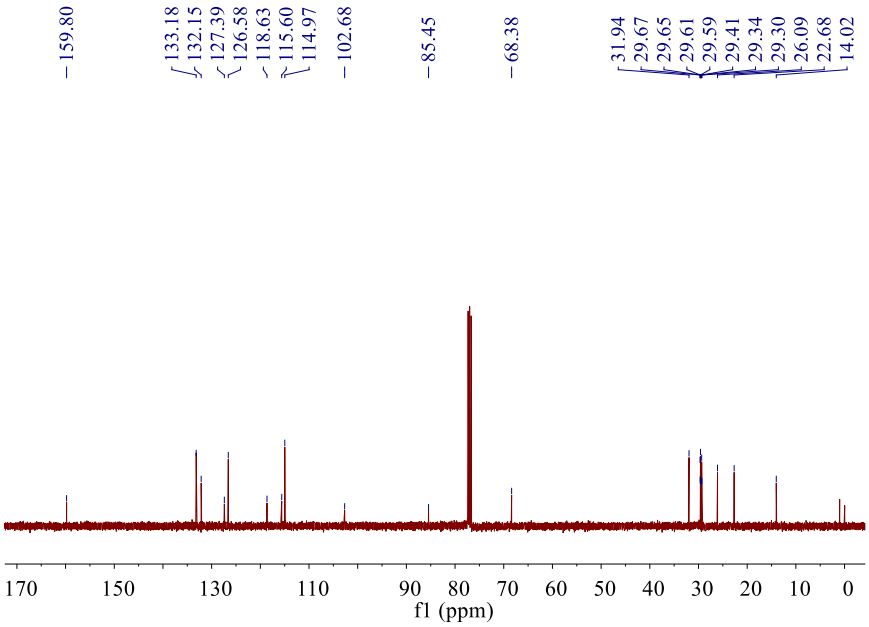

Figure S23. ^{13}C NMR spectrum (101 MHz, $CDCl_3$, 323 K) of **G0**.

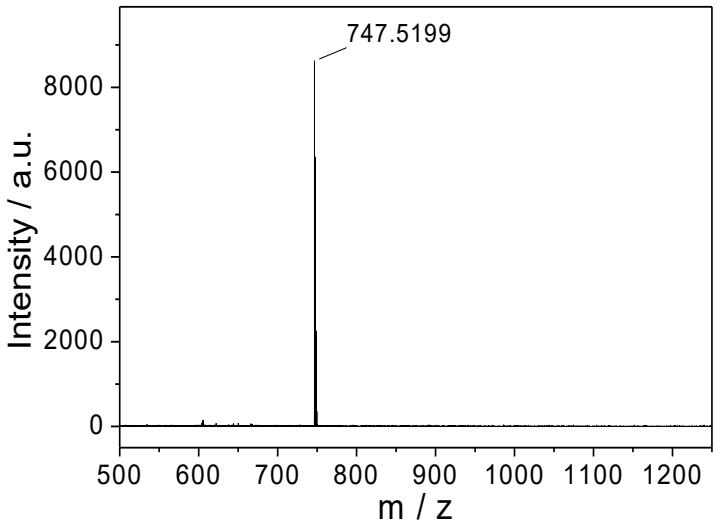

Figure S24. MALDI-TOF-MS spectrum of **G0**.

*5.2 Synthesis of compound **2***

Compound **3** (217 mg, 0.30 mmol), $Pd(PPh_3)_2Cl_2$ (21.0 mg, 0.03 mmol) and CuI (5.07 mg, 0.03 mmol) were mixed in 20 mL of TEA and stirred under nitrogen atmosphere. Trimethylsilylacetylene (147 mg, 1.50 mmol) was added dropwise to the reaction mixture over 30 minutes. After stirring at 55 ºC for 12 hours, the reaction mixture was evaporated to remove the solvent, and the residue was purified by flash column chromatography (petroleum ether/CH_2Cl_2, 10 : 1 *v*/*v* as the eluent) to afford the product as an oil liquid (203 mg, 93%). It was then treated with tetrabutylammonium

fluoride (219 mg, 0.84 mmol) in THF (20 mL) at 25 °C for 6 hours. After the deprotection reaction, the solvent was removed *in vacuo*, and the residue was extracted with H_2O/CH_2Cl_2. The combined organic extracts were dried over anhydrous Na_2SO_4 and evaporated with a rotary evaporator. The residue was purified by flash column chromatography (petroleum ether/CH_2Cl_2, 50: 1 *v*/*v* as the eluent) to afford compound **2** as a white solid (175 mg, 86 %). ^{1}H NMR (400 MHz, $CDCl_3$) δ (ppm): 7.31 (d, J = 7.7 Hz, 4H), 6.90 (d, J = 7.5 Hz, 4H), 6.72 (s, 2H), 6.60 (s, 1H), 4.93 (s, 4H), 3.95 (t, J = 6.4 Hz, 4H), 3.03 (s, 1H), 1.78 (dd, J = 13.8, 6.9 Hz, 4H), 1.44 (d, J = 7.5 Hz, 4H), 1.26 (s, 32H), 0.88 (t, J = 6.3 Hz, 6H).

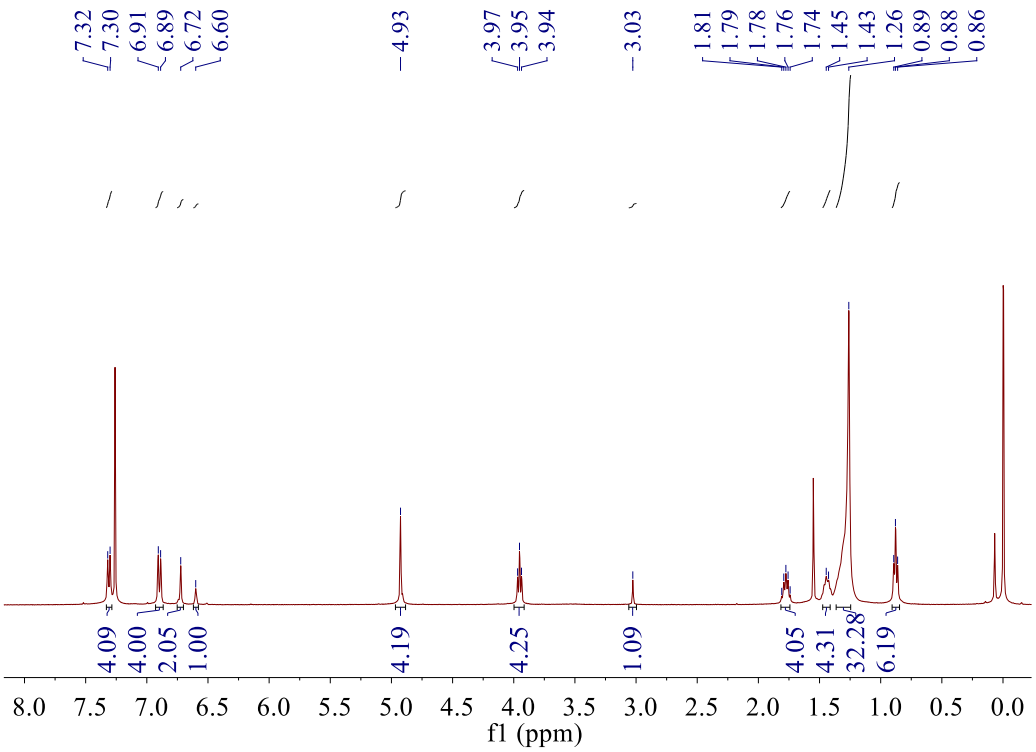

Figure S25. ^{1}H NMR spectrum (400 MHz, $CDCl_3$, 298 K) of compound **2**.

*5.3 Synthesis of dendrimer **G1***

9,10-diiodoanthracene (22.2 mg, 0.05 mmol), compound **2** (100 mg, 0.15 mmol), $Pd(PPh_3)Cl_2$ (14.0 mg, 0.02 mmol) and CuI (3.8 mg, 0.02 mmol) were mixed in TEA (20 mL) and stirred under nitrogen atmosphere. After stirring at 75 °C for 12 hours, the reaction mixture was evaporated to remove the solvent, and the residue was extracted with H_2O/CH_2Cl_2 for three times. The combined organic extracts were dried over

anhydrous Na_2SO_4, and the solvent was removed with a rotary evaporator. The residue was purified by flash column chromatography (petroleum ether/CH_2Cl_2, 10 : 1 *v*/*v* as the eluent) to afford dendrimer **G1** as an orange solid (45 mg, 58 %). ^{1}H NMR (400 MHz, $CDCl_3$) δ (ppm): 8.67 (dd, J = 6.6, 3.3 Hz, 4H), 7.64 (dd, J = 6.7, 3.2 Hz, 4H), 7.38 (d, J = 8.6 Hz, 8H), 7.01 (d, J = 2.2 Hz, 4H), 6.93 (d, J = 8.6 Hz, 8H), 6.69 (t, J = 2.2 Hz, 2H), 5.04 (s, 8H), 3.97 (t, J = 6.6 Hz, 8H), 1.82–1.76 (m, 8H), 1.47–1.42 (m, 8H), 1.29–1.24 (m, 64H), 0.89 (d, J = 6.6 Hz, 12H). ^{13}C NMR (101 MHz, $CDCl_3$) δ (ppm): 159.92, 159.15, 132.10, 129.39, 128.30, 127.23, 126.85, 124.60, 118.37, 114.61, 110.65, 103.42, 102.45, 86.10, 70.14, 68.05, 31.91, 31.42, 30.16, 29.65, 29.63, 29.59, 29.58, 29.40, 29.34, 29.24, 26.03, 22.68, 14.13. MALDI-TOF-MS *m*/*z*: $[M + H]^+$, $C_{106}H_{139}O_8$, calculated 1540.0470; found 1540.0391.

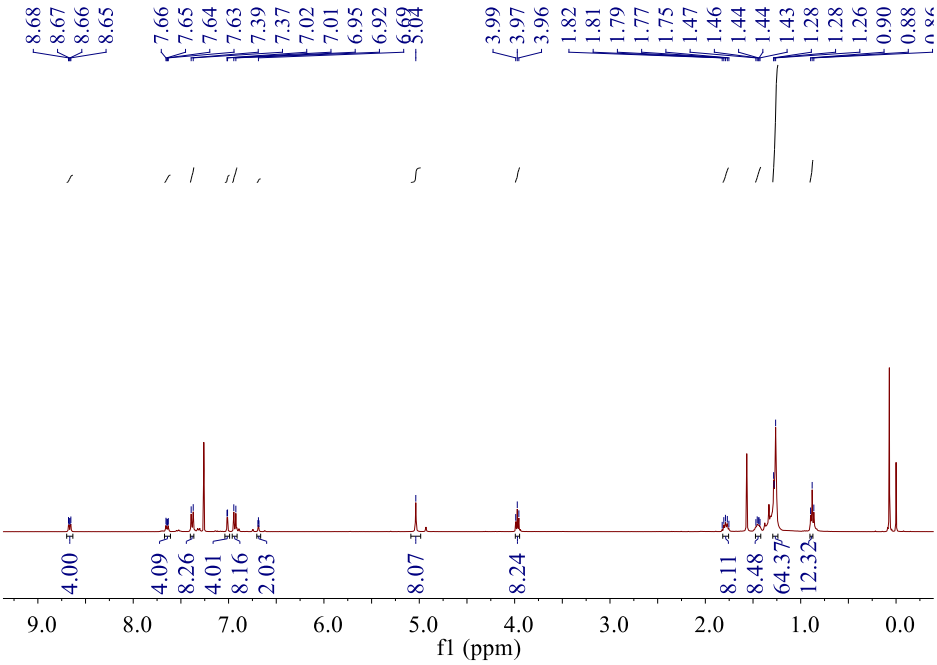

Figure S26. ^{1}H NMR spectrum (400 MHz, $CDCl_3$, 298 K) of dendrimer **G1**.

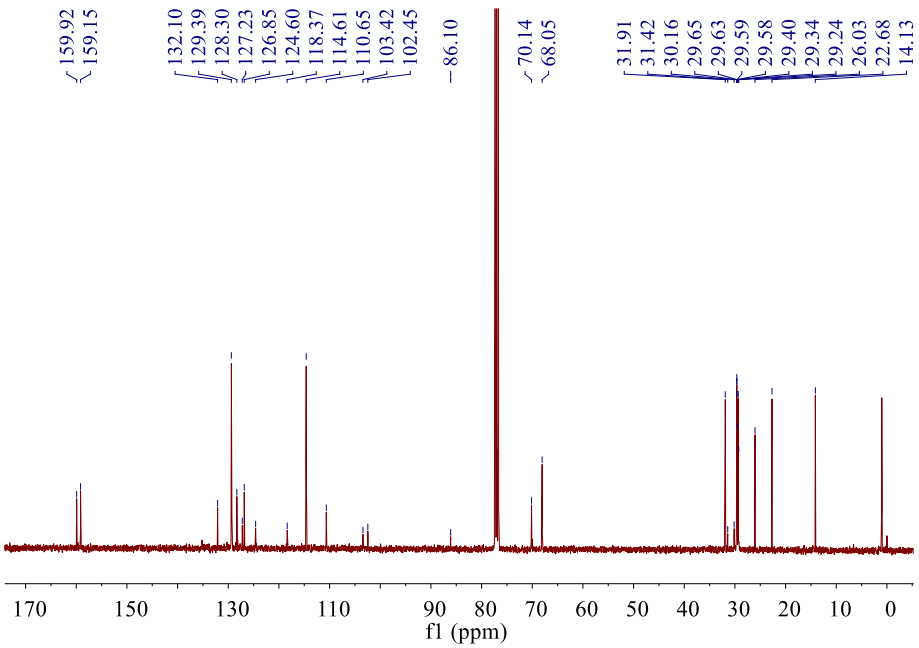

Figure S27. ^{13}C NMR spectrum (101 MHz, $CDCl_3$, 298 K) of dendrimer **G1**.

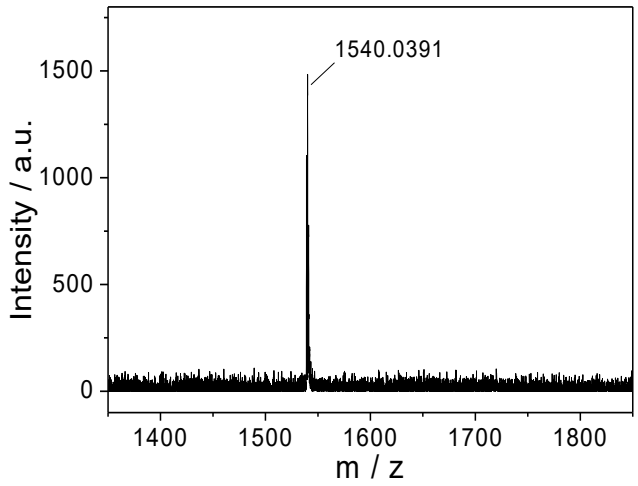

Figure S28. MALDI-TOF-MS spectrum of dendrimer **G1**.

*5.4 Synthesis of compound **8***

Compound **4** (313 mg, 0.50 mmol), methyl 3,5-dihydroxybenzoate (38.0 mg, 0.23 mmol) and K_2CO_3 (300 mg, 2.17 mmol) were added into 30 mL of DMF. After stirred at 80 °C for 12 hours, the solvent was evaporated under reduced pressure and the residue was extracted with H_2O/CH_2Cl_2 for three times. The combined organic extracts were dried over anhydrous Na_2SO_4 and the solvent was removed with a rotary evaporator. The residue was purified by flash column chromatography (petroleum ether/CH_2Cl_2, 20 : 1 *v/v* as the eluent) to afford compound **8** as a white solid (150 mg, 91 %). ^{1}H NMR

(400 MHz, $CDCl_3$) δ (ppm): 7.33 (d, J = 8.6 Hz, 4H), 7.28 (d, J = 2.3 Hz, 2H), 6.90 (d, J = 8.6 Hz, 4H), 6.77 (t, J = 2.3 Hz, 1H), 4.98 (s, 4H), 3.95 (t, J = 6.6 Hz, 4H), 3.90 (s, 3H), 1.77 (dd, J = 14.7, 6.8 Hz, 4H), 1.47–1.41 (m, 4H), 1.35–1.25 (m, 32H), 0.88 (t, J = 6.8 Hz, 6H).

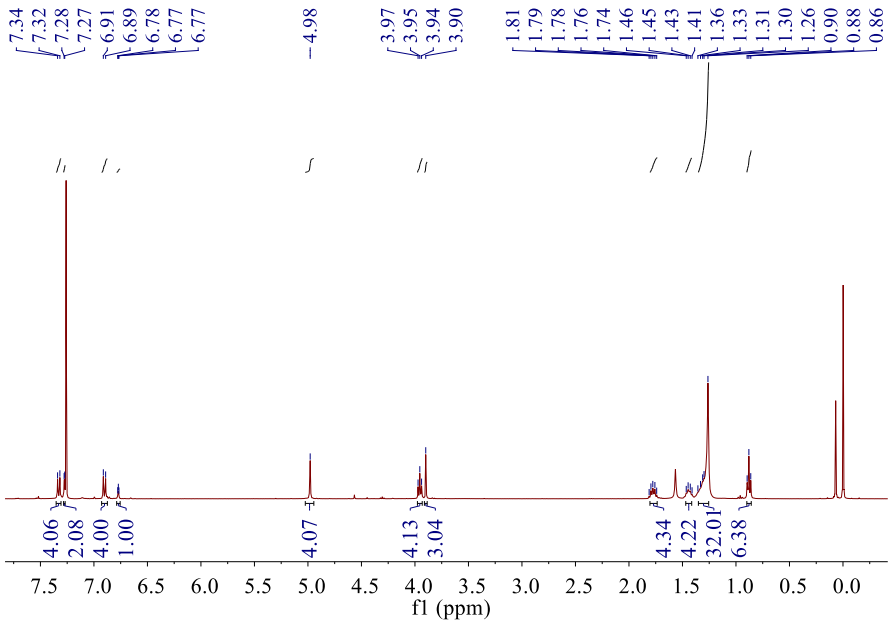

Figure S29. ^{1}H NMR spectrum (400 MHz, $CDCl_3$, 298 K) of compound **8**.

5.5 Synthesis of compound 7

Compound **8** (287 mg, 0.40 mmol) was added into 30 mL of THF and stirred under nitrogen atmosphere at 0 °C. $LiAlH_4$ (45.6 mg, 1.20 mmol) was then added dropwise to the reaction mixture over 30 minutes. After stirring at room temperature for 12 hours, the reaction mixture was quenched by methanol and the residue was extracted with H_2O/CH_2Cl_2 for three times. The combined organic extracts were dried over anhydrous Na_2SO_4, and the solvent was removed with a rotary evaporator. The residue was purified by flash column chromatography (petroleum ether/CH_2Cl_2, 10 : 1 *v/v* as the eluent) to afford compound **7** as a white solid (245 mg, 89 %). ^{1}H NMR (400 MHz, $CDCl_3$) δ (ppm): 7.33 (d, J = 8.6 Hz, 4H), 6.90 (d, J = 8.7 Hz, 4H), 6.61 (d, J = 2.2 Hz, 2H), 6.53 (t, J = 2.2 Hz, 1H), 4.95 (s, 4H), 4.63 (d, J = 4.4 Hz, 2H), 3.96 (t, J = 6.6 Hz, 4H), 1.77 (dd, J = 14.7, 6.8 Hz, 4H), 1.47–1.41 (m, 4H), 1.35–1.26 (m, 32H), 0.88 (d, J = 7.0 Hz, 6H).

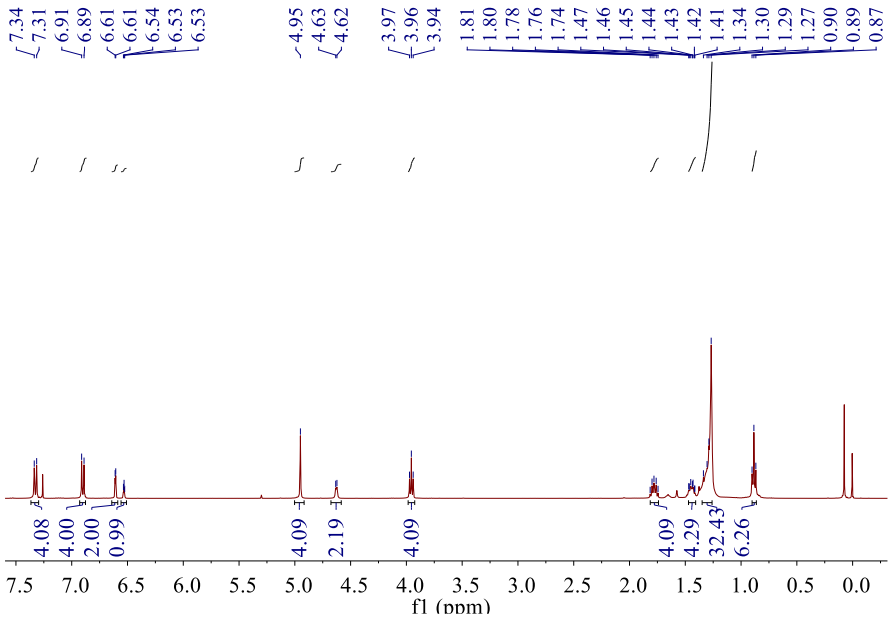

Figure S30. ^{1}H NMR spectrum (400 MHz, $CDCl_3$, 298 K) of compound **7**.

5.6 Synthesis of compound ***6***

Compound **7** (200 mg, 0.29 mmol) was added into 30 mL of CH_2Cl_2 and stirred under nitrogen atmosphere at 0 °C. 1 mL of $SOCl_2$ was added dropwise to the reaction mixture over 10 minutes. After stirring at room temperature for 6 hours, the reaction mixture was quenched by H_2O and the residue was extracted with H_2O/CH_2Cl_2 for three times. The combined organic extracts were dried over anhydrous Na_2SO_4, and the solvent was removed with a rotary evaporator. The residue was then mixed with $CsCO_3$ (156 mg, 0.48 mmol) and 5-bromoresorcinol (22.7 mg, 0.12 mmol) in MeCN (20 mL) and stirred at 25 °C for 12 hours. After the reaction was complete, the solvent was removed *in vacuo*, and the residue was extracted with H_2O/CH_2Cl_2. The combined organic extracts were dried over anhydrous Na_2SO_4 and evaporated with a rotary evaporator. The residue was purified by flash column chromatography (petroleum ether/CH_2Cl_2, 20 : 1 *v/v* as the eluent) to afford compound **6** as a white solid (138 mg, 75 %). ^{1}H NMR (400 MHz, $CDCl_3$) δ (ppm): 7.32 (d, J = 8.6 Hz, 8H), 6.89 (d, J = 8.6 Hz, 8H), 6.74 (d, J = 2.1 Hz, 2H), 6.63 (d, J = 2.1 Hz, 4H), 6.56 (d, J = 2.1 Hz, 2H), 6.51 (t, J = 2.1 Hz, 1H), 4.94 (d, J = 2.9 Hz, 12H), 3.95 (t, J = 6.6 Hz, 8H), 1.81–1.74 (m, 8H), 1.47–1.42 (m, 8H), 1.36–1.26 (m, 64H), 0.88 (t, J = 6.8 Hz, 12H).

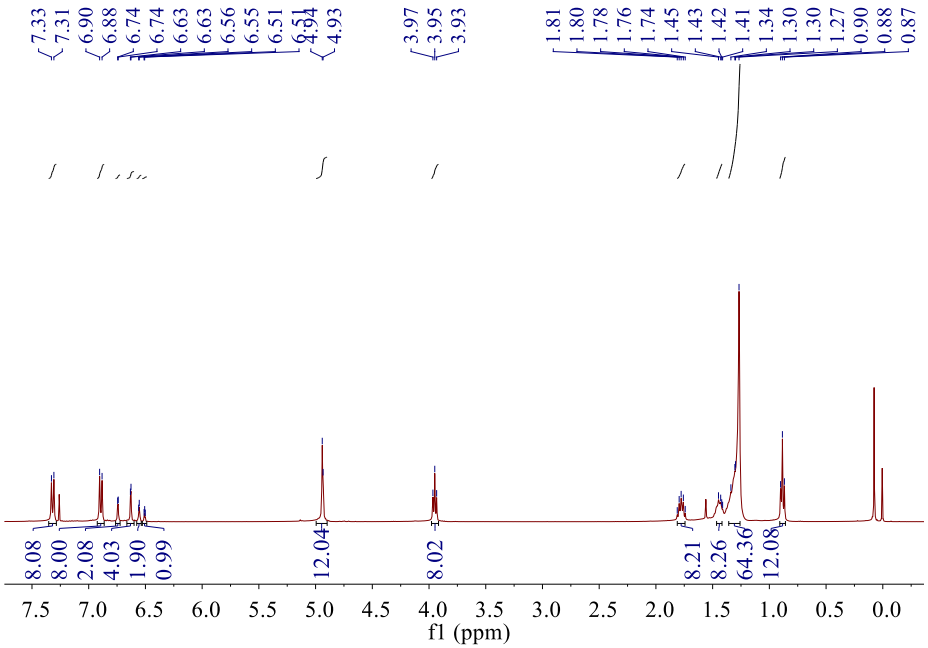

Figure S31. ^{1}H NMR spectrum (400 MHz, $CDCl_3$, 298 K) of compound **6**.

5.7 Synthesis of compound ***5***

Compound **6** (200 mg, 0.13 mmol), $Pd(PPh_3)_2Cl_2$ (14.0 mg, 0.02 mmol) and CuI (3.38 mg, 0.03 mmol) were mixed in 20 mL of TEA and stirred under nitrogen atmosphere. 2-Methyl-3-butyn-2-ol (200 mg, 2.38 mmol) was added dropwise to the reaction mixture over 30 minutes. After stirring at 80 ºC for 12 hours, the reaction mixture was evaporated to remove the solvent, and the residue was purified by flash column chromatography (petroleum ether/CH_2Cl_2, 10 : 1 *v/v* as the eluent) to afford the product as an oil liquid (155 mg, 78%). It was then treated with KOH (16.0 mg, 0.30 mmol) in toluene (20 mL) at 85 ºC for 6 hours. After the deprotection reaction, the solvent was removed, and the residue was extracted with H_2O/CH_2Cl_2. The combined organic extracts were dried over anhydrous Na_2SO_4 and evaporated with a rotary evaporator. The residue was purified by flash column chromatography (petroleum ether/CH_2Cl_2, 20 : 1 *v/v* as the eluent) to afford compound **5** as a white solid (127 mg, 85 %). ^{1}H NMR (400 MHz, $CDCl_3$) δ (ppm): 7.32 (d, J = 8.6 Hz, 8H), 6.89 (d, J = 8.6 Hz, 8H), 6.72 (d, J = 2.2 Hz, 2H), 6.64 (d, J = 2.1 Hz, 4H), 6.60 (t, J = 2.2 Hz, 1H), 6.55 (t, J = 2.1 Hz, 2H), 4.95 (d, J = 5.0 Hz, 12H), 3.95 (t, J = 6.6 Hz, 8H), 3.04 (s, 1H), 1.78 (dd, J = 14.3, 7.3 Hz, 8H), 1.47–1.42 (m, 8H), 1.28 (d, J = 15.5 Hz, 64H), 0.90–

0.88 (m, 12H).

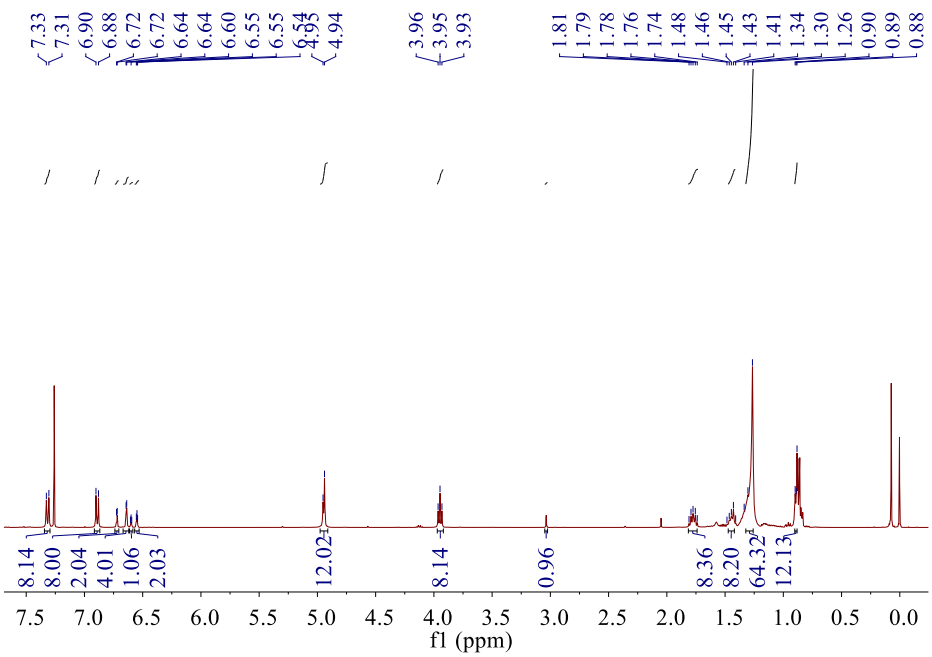

Figure S32. ^{1}H NMR spectrum (400 MHz, $CDCl_3$, 298 K) of compound **5**.

*5.8 Synthesis of dendrimer **G2***

9,10-diiodoanthracene (15.9 mg, 0.037 mmol), compound **5** (120 mg, 0.08 mmol), $Pd(PPh_3)_2Cl_2$ (9.80 mg, 0.04 mmol) and CuI (5.33 mg, 0.03 mmol) were stirred in TEA (20 mL) under nitrogen atmosphere. After stirring at 75 °C for 12 hours, the reaction mixture was evaporated to remove the solvent, and the residue was extracted with H_2O/CH_2Cl_2 for three times. The combined organic extracts were dried over anhydrous Na_2SO_4, and the solvent was removed with a rotary evaporator. The residue was purified by flash column chromatography (petroleum ether/CH_2Cl_2, 15 : 1 *v/v* as the eluent) to afford **G2** as an orange solid (93.7 mg, 81 %). ^{1}H NMR (400 MHz, $CDCl_3$) δ (ppm): 8.67 (dd, J = 6.7, 3.2 Hz, 4H), 7.63 (dd, J = 6.6, 3.2 Hz, 4H), 7.32 (d, J = 8.6 Hz, 16H), 7.01 (d, J = 2.2 Hz, 4H), 6.89 (d, J = 8.7 Hz, 16H), 6.71 (d, J = 2.1 Hz, 8H), 6.68 (t, J = 2.1 Hz, 2H), 6.58 (t, J = 2.1 Hz, 4H), 5.06 (s, 8H), 4.96 (s, 16H), 3.93 (t, J = 6.6 Hz, 16H), 1.77 (dd, J = 14.2, 7.3 Hz, 16H), 1.59 (s, 16H), 1.42 (d, J = 7.5 Hz, 16H), 1.25 (s, 112H), 0.87 (t, J = 6.8 Hz, 24H). ^{13}C NMR (101 MHz, $CDCl_3$) δ (ppm): 160.25, 159.79, 159.05, 138.84, 132.11, 129.31, 128.47, 127.21, 126.92, 124.68, 118.34, 114.54, 110.78, 106.29, 103.39, 102.38, 101.62, 86.23, 70.20, 69.94, 68.01, 31.90,

29.65, 29.62, 29.59, 29.57, 29.39, 29.34, 29.23, 26.02, 22.68, 14.12. MALDI-TOF-MS *m/z*: $[M + H]^+$, $C_{210}H_{283}O_{20}$, calculated 3125.1128; found 3125.0681.

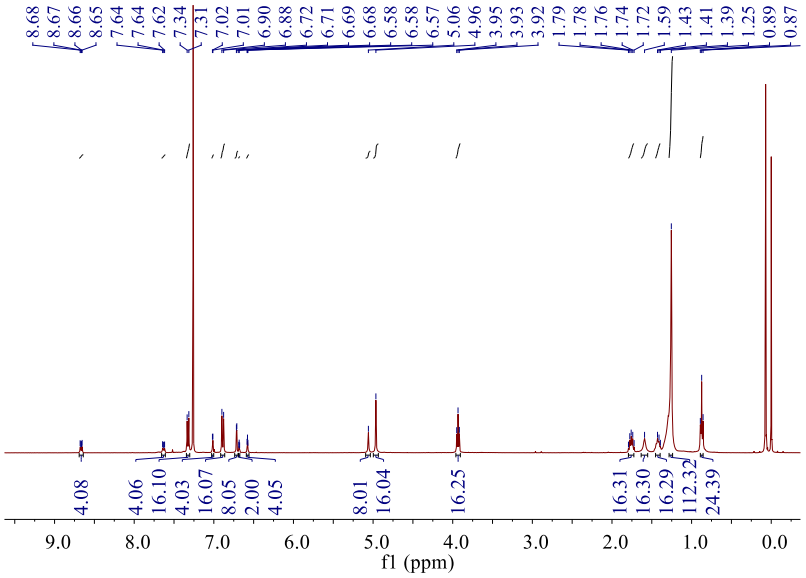

Figure S33. ^{1}H NMR spectrum (400 MHz, $CDCl_3$, 298 K) of dendrimer **G2**.

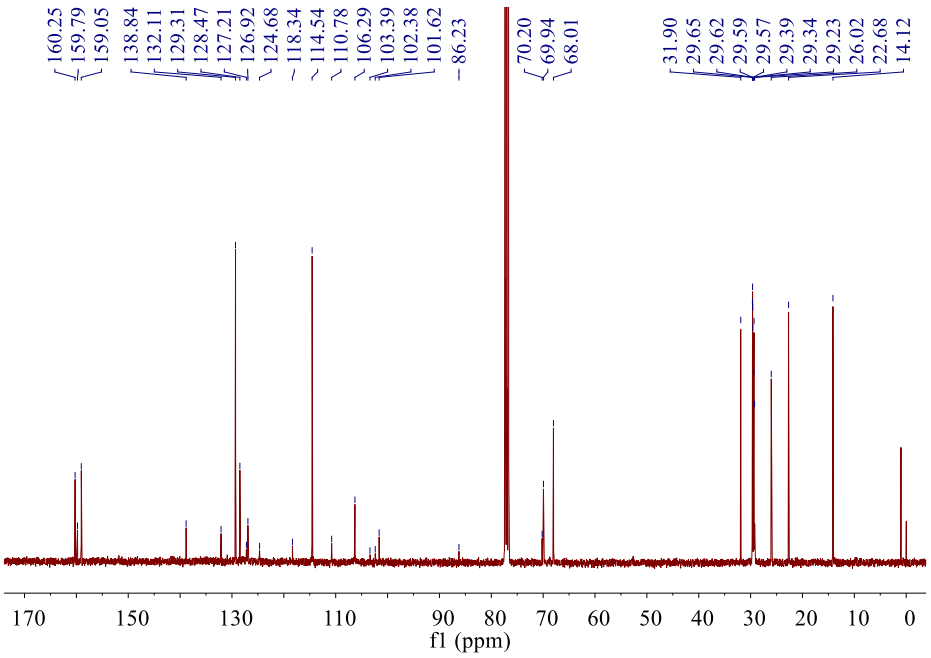

Figure S34. ^{13}C NMR spectrum (101 MHz, $CDCl_3$, 298 K) of dendrimer **G2**.

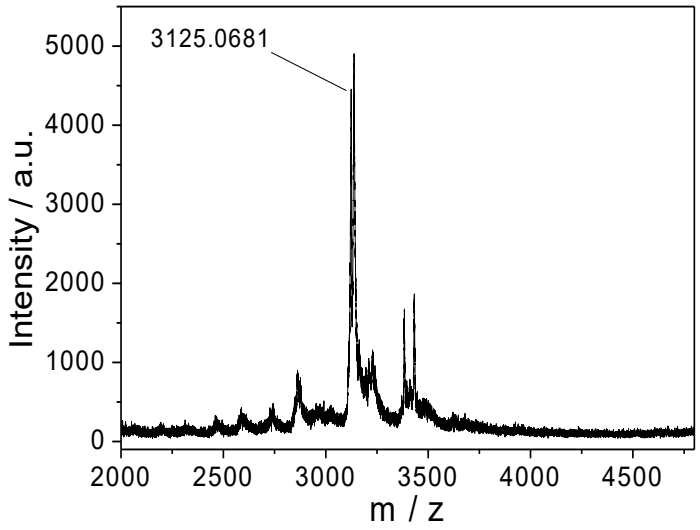

Figure S35. MALDI-TOF-MS spectrum of dendrimer **G2**.

References

S1. M. Lebtow, I. Helmers, V. Stepanenko, R. Q. Albuquerque, T. B. Marder, G. Fernández. *Chem. Eur. J.*, 2017, **23**, 6198.

S2. G. M. Plante, D. Fortin, A. Soldera, Pierre D. Harvey. *Organometallics*, 2018, **37**, 2544.

S3. B. T. Diroll, D. Jishkariani, M. Cargnello, C. B. Murray, B. Donnio. *J. Am. Chem. Soc*., 2016, **138**, 10508.

S4. Gaussian 09, Revision A.02, M. J. Frisch, G. W. Trucks, H. B. Schlegel, G. E. Scuseria, M. A. Robb, J. R. Cheeseman, G. Scalmani, V. Barone, B. Mennucci, G. A. Petersson, H. Nakatsuji, M. Caricato, X. Li, H. P. Hratchian, A. F. Izmaylov, J. Bloino, G. Zheng, J. L. Sonnenberg, M. Hada, M. Ehara, K. Toyota, R. Fukuda, J. Hasegawa, M. Ishida, T. Nakajima, Y. Honda, O. Kitao, H. Nakai, T. Vreven, J. A. Montgomery, Jr., J. E. Peralta, F. Ogliaro, M. Bearpark, J. J. Heyd, E. Brothers, K. N. Kudin, V. N. Staroverov, R. Kobayashi, J. Normand, K. Raghavachari, A. Rendell, J. C. Burant, S. S. Iyengar, J. Tomasi, M. Cossi, N. Rega, J. M. Millam, M. Klene, J. E. Knox, J. B. Cross, V. Bakken, C. Adamo, J. Jaramillo, R. Gomperts, R. E. Stratmann, O. Yazyev, A. J. Austin, R. Cammi, C. Pomelli, J. W. Ochterski, R. L. Martin, K. Morokuma, V. G. Zakrzewski, G. A. Voth, P. Salvador, J. J. Dannenberg, S. Dapprich, A. D. Daniels,O. Farkas, J. B. Foresman, J. V. Ortiz, J. Cioslowski, and D. J. Fox, *Gaussian, Inc.,*

Wallingford CT, 2009.

S5. P. Jonkheijm, P. van der Schoot, A. P. H. J. Schenning, E. W. Meijer, *Science,* 2006, **313**, 80.

S6. M. M. J. Smulders, M. K. L. Nieuwenhuizen, T. F. A. de Greef, P. van der Schoot, A. P. H. J. Schenning, E. W. Meijer, *Chem. Eur. J.,* 2010, **16**, 362.

S7. P. A. Korevaar, C. Schaefer, T. F. A. de Greef, E. W. Meijer, *J. Am. Chem. Soc.,* 2012, **134**, 13482.